



# Microstructures and superconducting properties of MgB<sub>2</sub> bulk samples processed by ultra-high pressure-assisted sintering

Zilin Gao<sup>a</sup>, Sangeeta Santra<sup>a,b</sup>, Sajjad Amirkhanlou<sup>a</sup>, Edwin Eardley<sup>c,d</sup>, Chris Wort<sup>c</sup>, Chris R.M. Grovenor<sup>a</sup>, Susannah C. Speller<sup>a,\*</sup>

<sup>a</sup> Department of Materials, University of Oxford, Parks Road, OX1 3PH, United Kingdom

<sup>b</sup> Department of Material Science and Engineering, Indian Institute of Technology Delhi, Delhi 110016, India

<sup>c</sup> Element Six, Global Innovation Centre, Fermi Avenue, Harwell Oxford, Didcot, Oxfordshire OX11 0QR, United Kingdom

<sup>d</sup> United Kingdom Atomic Energy Authority, Culham Science Centre, Abingdon, Oxfordshire OX14 3DB, United Kingdom

## ARTICLE INFO

### Keywords:

MgB<sub>2</sub> bulk samples  
Ultra-high pressure sintering  
Crystal defects  
Grain refinement  
High magnetic fields

## ABSTRACT

Nanocrystalline MgB<sub>2</sub> bulk superconductors have been fabricated by ultra-high pressure-assisted sintering (~ 5 GPa) over a range of temperatures (700 °C–1100 °C). Phase evolution and morphology, grain size and lattice defects were systematically investigated. The superconducting performance was measured using magnetization methods and linked to the corresponding microstructural features. A sample processed at 900 °C and 5 GPa achieved a J<sub>c</sub> value of 4.5 × 10<sup>7</sup> A/m<sup>2</sup> at 4.2 K, 6 T, 30 times and more than 100 times higher than those prepared at 800 and 1100 °C respectively, under similar pressures. Its superior superconducting properties arise from the combination of limited grain growth, retained crystal defects and complete densification achieved in a rapid process by the application of ultra-high pressure. This study reveals the importance of microstructure in controlling the superconducting behavior in sintered MgB<sub>2</sub>, especially the sample homogeneity that can affect the length scales over which the supercurrents flow.

## 1. Introduction

Bulk superconductors can trap higher magnetic fields than permanent magnets, making them potentially interesting for applications such as limb-scale magnetic resonance imaging (MRI), magnetic drug targeting and magnetic separation [1]. Magnesium diboride (MgB<sub>2</sub>) has the highest critical transition temperature (T<sub>c</sub> = 39 K) of conventional superconductors at ambient pressure [2], and so is well suited for use with a compact, liquid helium-free cryocooler to reduce both cryostat size and operating cost [2,3]. Unlike REBCO superconductors, the grain boundaries in MgB<sub>2</sub> are effective pinning sites and not weak links [4,5], so high J<sub>c</sub> values can be achieved in polycrystalline bulks by cheap and easy powder processing techniques.

There are two ways to improve the trapped field (B<sub>trap</sub>) in superconducting bulk magnets; (i) improving the macroscopic critical current density (macro J<sub>c</sub>) circulating in the superconductors, and (ii) increasing the radial (and to a lesser extent, axial) dimension over which it circulates. B<sub>trap</sub> is predicted by numerical analysis to reach saturation with an increase in sample diameter [6], so improving J<sub>c</sub>(B) values of bulk

superconductors becomes the most effective way of enhancing B<sub>trap</sub>.

Obtaining high J<sub>c</sub> values over macroscopic length scales in bulk samples requires strong pinning within the grains to obtain high intra-granular J<sub>c</sub> (here termed micro J<sub>c</sub>), as well as good current flow between grains. As shown in Fig. 1, in addition to the intrinsic superconducting properties such as T<sub>c</sub> and B<sub>c2</sub>, the local J<sub>c</sub> values are sensitive to the microstructural flux pinning landscape. Grain boundary pinning has been demonstrated to be the main pinning mechanism in polycrystalline MgB<sub>2</sub> [7], so achieving a fine grain size is an effective way to improve performance. High energy ball milling is widely used to refine crystallite size and to create lattice strain, leading to high critical current densities and therefore outstanding B<sub>trap</sub> performance [8–10]. Some second phase impurities resulting from chemical doping can also retard grain growth at high processing temperatures leading to effective flux pinning landscapes created by a fine grain size [11].

However, to enable current flow around the whole of a bulk MgB<sub>2</sub> sample, both high density and good grain connectivity are required [12]. Connectivity is influenced in a complex way by the mechanisms by which the microstructure is developed. For example, the presence of

\* Correspondence to: Department of Materials, Parks Road, Oxford, OX1 3PH  
E-mail address: [susannah.speller@materials.ox.ac.uk](mailto:susannah.speller@materials.ox.ac.uk) (S.C. Speller).

<https://doi.org/10.1016/j.jeurceramsoc.2022.09.008>

Received 30 May 2022; Received in revised form 1 September 2022; Accepted 4 September 2022

Available online 7 September 2022

0955-2219/© 2022 The Author(s). Published by Elsevier Ltd. This is an open access article under the CC BY license (<http://creativecommons.org/licenses/by/4.0/>).

porosity or non-superconducting secondary phases will clearly reduce the cross-section area for current transport. The distribution of these secondary phases or pores is also of crucial importance; small, isolated non-superconducting defects have much less impact than secondary phases decorating grain boundaries that can if too numerous form semi-continuous barriers to current flow. Less obvious is the contribution of the anisotropy in  $H_{c2}$  values in  $MgB_2$  ( $H_{c2}^{||ab}/H_{c2}^{||c}$ ) on current percolation in polycrystalline  $MgB_2$ . As discussed in detail by Eisterer et al. [13], as the applied field increases, grains aligned unfavorably with respect to the field become normal, leading to a decrease in the current carrying cross-section. As a result, the texture (preferred crystallographic alignment) of  $MgB_2$  grains is also an important parameter.

By changing processing methods or sintering conditions, one can control the microstructure and thus optimize the superconducting performance of bulk samples. In-situ processing of  $MgB_2$  bulks (using Mg and B powders to make the green compact, followed by a reaction at temperatures usually  $<900^\circ\text{C}$  to form the  $MgB_2$  phase) tends to result in good quality interfaces between grains, but the bulk samples suffer from inherent porosity as a result of the volume contraction associated with the reaction to form  $MgB_2$  [14]. In contrast, sintering pre-reacted  $MgB_2$  powder at temperatures typically  $>900^\circ\text{C}$  enables high densities to be achieved in ex-situ techniques, especially with the assistance of pressures by spark plasma sintering (50–100 MPa) [15–19]. Ultra-high pressure-assisted sintering ( $>2$  GPa) is widely used in producing nano-structured ferroelectric ceramics and dense engineering ceramics, with the aim of achieving high bulk densities at lower sintering temperatures [20–24]. By investigating the role of extreme pressure (5 GPa) on processing other bulk samples such as alumina, it is also found that plastic deformation can aid the elimination of pores and enhance local atomic diffusion at grain boundaries, which helps achieve bulk densification in short process times [25]. High pressure synthesis of  $MgB_2$  bulk samples by both in-situ and ex-situ methods has been carried out in various studies [26–29], but the superconducting behaviour of the ex-situ samples in particular is not very consistent, nor has a systematic explanation of the link between processing temperatures, microstructures and superconducting properties been reported. Here we have examined the effect of temperature on the microstructural evolution of ex-situ  $MgB_2$  bulk samples processed by ultra-high pressure-assisted sintering. This study linking microstructural evolution to the corresponding changes in superconducting performance may also have implications for optimising the properties of polycrystalline superconductors processed by other methods.

## 2. Experimental details

All our samples were prepared from commercial  $MgB_2$  powders (purity: 99%, Alfa Aesar) using processing facilities at Element Six designed for the production of artificial diamond components [30]. An

industrial scale cubic press was used to apply pressures of 5–5.5 GPa at temperatures ranging from  $700^\circ\text{C}$  to  $1100^\circ\text{C}$ . Detailed processing conditions for all the samples are shown in Table 1. In addition, samples processed under 5.5 GPa and at  $800^\circ\text{C}$  but with the sintering time varying from 5 to 20 min were prepared to provide Supplementary information on the stages of microstructural evolution.

Phase identification and quantitative analysis were carried out with X-ray diffraction (XRD) using  $\text{Cu-K}\alpha$  radiation of 0.154 nm at 40 kV and 40 mA (PANalytical Empyrean diffractometer). Phase fraction, lattice parameters, crystallite size and micro strain were obtained by Rietveld refinement (PANalytical HighScore Plus software). Microstructural evolution and composition were characterized using a Zeiss Merlin field-emission scanning electron microscope (FE-SEM) equipped with an Oxford Instruments 150 mm<sup>2</sup> Xmax EDX detector. The micro-texture was examined using a Zeiss Merlin FEG-SEM with Bruker electron back-scattered diffraction (EBSD) camera, and the data acquisition was performed using Esprit software. An accelerating voltage and beam current of 20 kV and 15 nA respectively were used in the data collection. The same SEM instrument equipped with a Bruker e-flash high-resolution EBSD detector and an OPTIMUS™ TKD head was used for Transmission Kikuchi Diffraction (TKD) analysis. ESPRIT 2.0 software was used for diffraction pattern collection, and post-processing was conducted by HKL Channel 5 software. A misorientation angle of  $15^\circ$  was chosen to define high angle grain boundaries. Transmission electron microscopy bright field (BF-TEM) observations, high resolution TEM (HRTEM) and scanning transmission electron microscopy (STEM) was performed in a JEOL JEM-3000 F operating at 300 kV.

Magnetic properties were measured using a 16 T Quantum Design Physical properties measurement system (PPMS) with a vibrating sample magnetometer (VSM). The sample size for PPMS was about  $2 \times 2 \times 3$  mm. The critical temperature ( $T_c$ ) was determined as the onset of superconductivity by moment-temperature sweeps at 5 mT. DC susceptibility was calculated by considering the size and shape of the sample,  $\chi_{\text{eff}} = \frac{\chi}{1+n\chi}$ , where  $\chi$  is the local material property and  $\chi_{\text{eff}}$  is the effective susceptibility taking into account demagnetization effects. The demagnetisation factor,  $n$ , is related to the geometry of the samples, and  $n \approx \frac{4ab}{4ab+3c(a+b)}$  for the cuboid samples in this study, where  $a$ ,  $b$  are the dimensions of the cross section ( $b > a$ ) and  $c$  is the dimension parallel to the applied field [31]. Moment-field (M-H) sweeps were taken at 4.2 K

**Table 1**  
Processing conditions of  $MgB_2$  bulk samples.

Sample	Time (min)	Temperature ( $^\circ\text{C}$ )	Pressure (GPa)
T700	15	700	5.5
T800	15	800	5.5
T900	15	900	5
T1100	15	1100	5

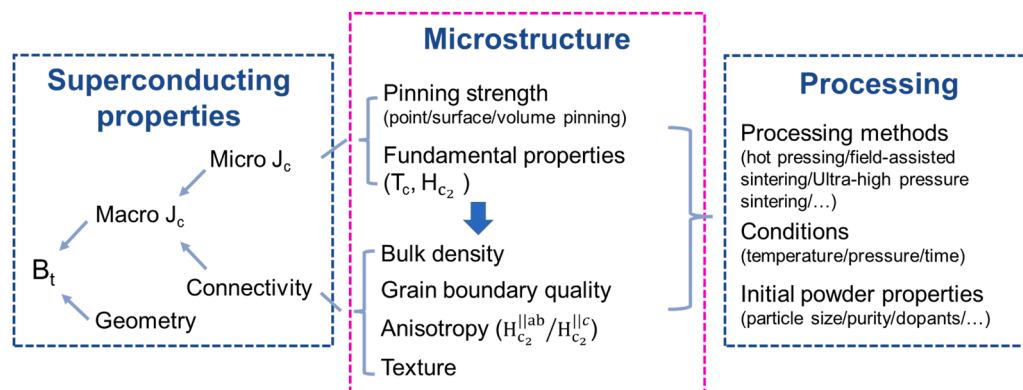


**Fig. 1.** Schematic of methods to improve the trapped field performance of  $MgB_2$  bulk superconductors.

and 20 K, and critical current density values calculated by Bean's critical state model,  $J_c = \frac{2\Delta M}{a(1-a/3b)}$ .

### 3. Results and discussion

#### 3.1. Analysis of X-ray diffraction patterns

X-ray diffraction (XRD) patterns for bulk samples processed between 900 °C and 1100 °C are presented in Fig. 2. All samples show evidence of the normal  $\text{MgB}_2$  decomposition products,  $\text{MgB}_4$  and  $\text{MgO}$  by the reaction  $2\text{MgB}_2(\text{s}) \rightleftharpoons \text{MgB}_4(\text{s}) + \text{Mg}(\text{l}, \text{g})$  [32]. As the processing temperature increases, one can observe the increasing intensity and decreasing full-width at half-maximum (FWHM) of  $\text{MgB}_2$  peaks, indicating an improvement in crystal quality. The enlarged figure highlights the (002) and (110) peaks, the angular positions of which are related to *c* and *a* axis of the  $\text{MgB}_2$  unit cell respectively. A clear shift of both peaks to lower angles with increasing sintering temperature from 700 °C to 900 °C corresponds to an increase in both *c* and *a* lattice parameters. The reference values of *a* and *c* parameters of pure  $\text{MgB}_2$  are 3.086 Å and 3.524 Å, respectively [33]. It can be seen that our *c* parameters approach the reference value at higher processing temperatures (Table 2). This increase in lattice parameters suggests the reduction in the inhomogeneous strains introduced by plastic deformation, which is also reflected in the reduction in peak broadening, as shown in Fig. 2. The peak splitting observed in T1100 is consistent with the expected  $\text{Cu K}_{\alpha 1}$  and  $\text{K}_{\alpha 2}$  X-ray contributions that are hidden by peak broadening in the samples processed at lower temperatures.

Table 2 summarises the results of quantitative analysis of the phase content by the Rietveld method. The software/procedure used for the Rietveld fitting methodology is the same as the analysis in [17], so the XRD results from  $\text{MgB}_2$  bulk samples processed by the field-assisted sintering technique (FAST) at 900 °C and 1100 °C are also listed in Table 2 for comparison. The  $\text{MgO}$  content is found to increase by around 5 wt. %, reaching 12 wt. % at the highest processing temperature of 1100 °C. An increase is also seen in  $\text{MgB}_4$  content, from 6 wt% in T700 to 13 wt% in T1100, although this is not as severe as the increase seen in the FAST samples processed at much lower pressure.

There is general agreement in the binary Mg-B system that, at conventional processing pressures up to 100 MPa,  $\text{MgB}_2$  will decompose to boride-rich phases such as  $\text{MgB}_4$  and  $\text{MgB}_7$  at higher temperatures, though the accurate decomposition temperatures are difficult to determine because of the high volatility of Mg [34]. Kim et al. recalculated

**Table 2**

The phase content, lattice parameters, crystallite size and strain obtained by Rietveld refinement. Refinement results from FAST samples are presented as a comparison, and the precision (defined as half the difference between the maximum and minimum values from 5 samples prepared under the same conditions) estimated as described in [17].

Sample	MgO (wt %)	MgB <sub>4</sub> (wt%)	MgB <sub>2</sub> a axis (Å)	MgB <sub>2</sub> c axis (Å)	Crystallite size (nm)	Micro strain (%)
T700	7	6	3.086	3.519	29	0.40
T800	8	6	3.086	3.519	30	0.37
T900	11	6	3.087	3.521	38	0.23
T1100	12	13	3.086	3.521	113	0.03
FAST900	7	11	3.085	3.525	120	0.12
FAST1100	8	16	3.084	3.527	140	0.13
Estimated error	±0.4	±1.1	±0.0002	±0.0003	±12	±0.005

the Mg-B phase diagram under external pressures varying from 1 atm to 100 MPa using the thermodynamic properties of magnesium borides [35]. A significant change in their theoretical Mg-B diagram under 100 MPa is the disappearance of the Mg gaseous phase below 3000 °C. They pointed out that an increase in external pressure can lead to a higher decomposition temperature for  $\text{MgB}_2/\text{MgB}_4$  since the boiling point of Mg increases. Therefore, Mg loss can be avoided and  $\text{MgB}_2$  decomposition can be suppressed at high ambient pressures, which may be important in the design of practical processing strategies. However, Bohnenstiehl et al. [34] experimentally determined that the temperature at which the reaction  $\text{MgB}_2 \rightarrow \text{L} + \text{MgB}_4$  occurred at 10 MPa was around 300 °C lower than the theoretical prediction (1740 °C) [35], which may indicate that  $\text{MgB}_2$  decomposition is much more likely to occur at low external pressures than calculations suggest. Our results show, as expected, that  $\text{MgB}_2$  becomes more unstable with increasing processing temperatures, but also that the thermodynamic stability of the superconducting phase has been improved by the application of very high pressures (~ 5 GPa) compared with the lower pressure FAST samples.

Dramatic crystallite growth only occurs when the temperature rises to 1100 °C, below which there is only a modest increase in  $\text{MgB}_2$  crystallite size (29 nm in T700 compared to 38 nm in T900). Even so, these values of crystallite size are still much smaller than those in samples prepared at the same nominal temperatures by FAST, a process in which only 50 MPa of pressure was applied for 5 min (Table 2). This

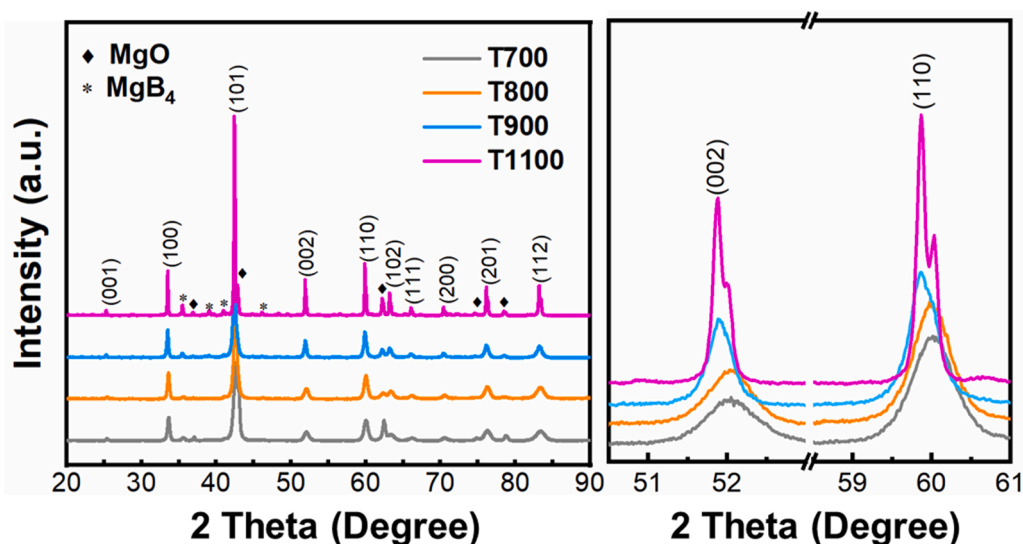


**Fig. 2.** X-ray diffraction (XRD) patterns of  $\text{MgB}_2$  samples processed at 700 °C, 800 °C, 900 °C and 1100 °C. The right figure shows an expanded region around the (002) and (110) peaks of  $\text{MgB}_2$ .



demonstrates the advantage of ultra-high pressure in retarding crystallite growth during sintering. The microstrain shows a steady drop from 0.4% in T700 to nearly zero in T1100, suggesting that inhomogeneous strains have been gradually eliminated at the higher processing temperatures.

### 3.2. Microstructural characterization

Backscattered scanning electron (BSE) images of two typical microstructures are shown in Fig. 3. MgO grains appear brighter than the MgB<sub>2</sub> matrix, and MgB<sub>4</sub> grains are darkest as a result of atomic number contrast. The T1100 sample in Fig. 3a shows dense polycrystalline MgB<sub>2</sub> regions ranging in size from a few microns to tens of microns, surrounded by MgB<sub>4</sub> and MgO grains. The relatively uniform grain structure inside these regions can be seen because of channeling effects in the backscattered electron images. Fig. 3b shows a lower temperature sample, T800, in which both dense and porous MgB<sub>2</sub> regions are distinguishable, as well as large MgB<sub>4</sub> grains. Fig. 3c is a high magnification image of a dense region in the T800 sample, highlighting bright MgO impurities at grain boundaries. The porous matrix in Fig. 3d contains a large number of partially-connected pores at the interfaces between MgB<sub>2</sub> particles, indicating incomplete densification.

Fig. 4 presents the microstructural evolution of samples processed under 5.5 GPa and at 800 °C but with the sintering time varying from 5 to 20 min. The most obvious microstructural change is the growth of the MgB<sub>4</sub> particles with time. At the beginning of processing (<5 min), there are a large number of pores in the samples, and dense regions can hardly be distinguished (Fig. 4a). As the time is extended to 10 min, a duplex microstructure forms, with dense MgB<sub>2</sub> regions surrounded by a porous matrix (Fig. 4c). Even after 20 min at this relatively low temperature, porous regions still exist (Fig. 4e). Close inspection shows there are

fewer pores in the dense MgB<sub>2</sub> regions than in the matrix, with a size of around 0.5 μm in t5 (Fig. 4b). These pores shrink and are almost completely eliminated in t10 and t20 samples, accompanied by the formation of a larger amount of fine MgO at the MgB<sub>2</sub> grain triple junctions (Fig. 4d and f). However, elongating the dwell time will aggravate MgB<sub>2</sub> decomposition and lead to the formation of larger MgB<sub>4</sub> grains rather than consolidation of the superconducting matrix.

SEM images of polished T700, T800, T900 and T1100 samples at different magnifications (500× and 3000×) are presented in Fig. 5. T700 has a high fraction of interconnected, non-uniform pores (Fig. 5a and b). As the temperature increases to 800 °C, dense MgB<sub>2</sub> regions up to 50 μm can be distinguished from a MgB<sub>2</sub> matrix that is porous and contains large MgB<sub>4</sub> impurity particles (Fig. 5c). The porous matrix is fully eliminated in T900 and T1100 samples, as shown in Fig. 5e and g, suggesting that complete densification can be achieved if the high-pressure sintering temperature is above 900 °C. The higher magnification images in Fig. 5f and h show that two different morphologies are present after processing at higher temperatures. i.e., well-connected regions with coarse grains separated by transition zones characterised by finer grains. These transition zones seem to be the final, and most difficult, regions to densify. However, some significant differences in microstructure distinguish the T1100 and T900 samples. First, the higher temperature leads to the formation of MgB<sub>9</sub> particles around 4 μm in size (Fig. 5g and Supplementary Fig. S1), as well as smaller, isolated MgB<sub>4</sub> grains. As Fig. 3a shows, these MgB<sub>4</sub> grains surrounding dense MgB<sub>2</sub> regions in T1100 form a partial barrier separating dense MgB<sub>2</sub> colonies from each other and thus decreasing connectivity, which we expect to be detrimental to the transport of macroscopic currents. The MgO-rich area in T1100 is a result of the severe decomposition of MgB<sub>2</sub>, and also indicates 1100 °C is above the optimal processing temperature.

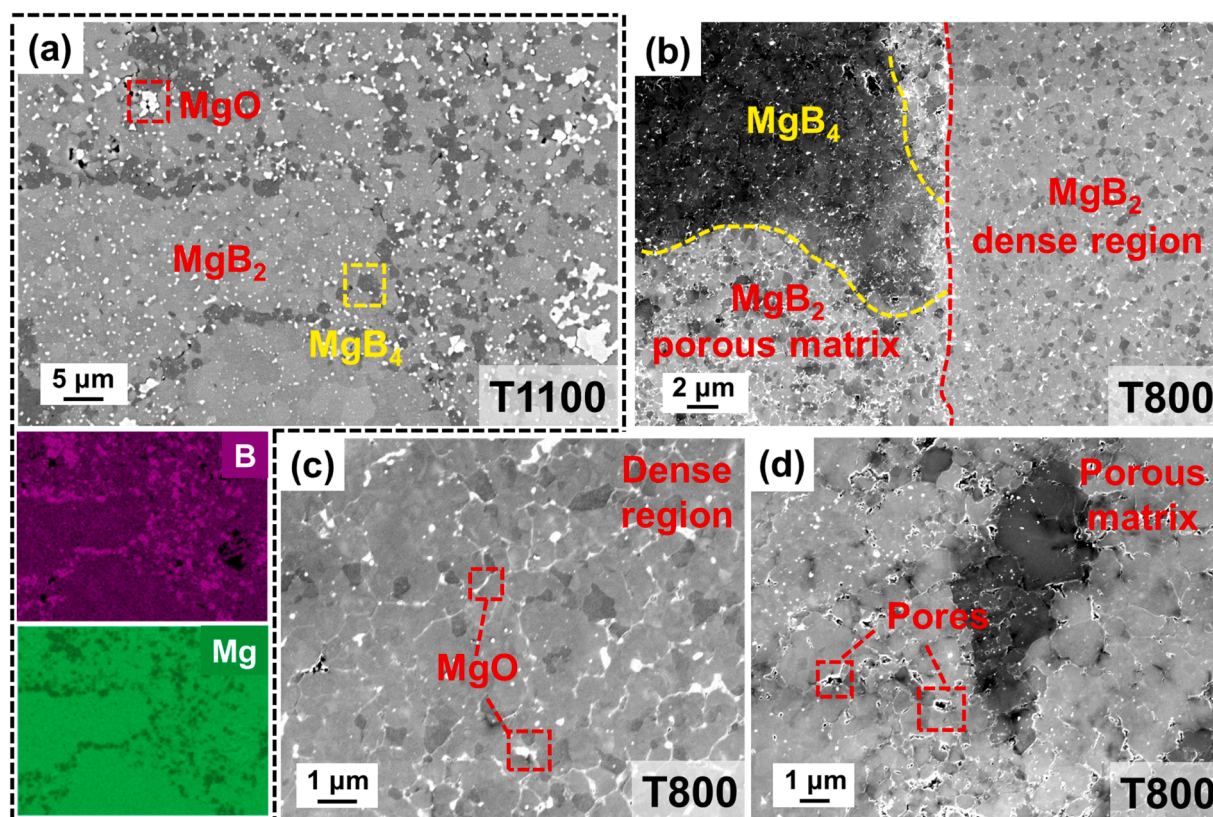


**Fig. 3.** Backscattered scanning electron (BSE) micrographs showing (a) the different contrast allowing identification of MgB<sub>2</sub>, MgO and MgB<sub>4</sub> (confirmed by the EDX maps for the distribution of Mg, B and O) in the sample processed at 1100 °C and 5 GPa for 15 min, and (b) the existence of dense MgB<sub>2</sub> regions, porous MgB<sub>2</sub> matrix and large MgB<sub>4</sub> phases in a sample processed at 800 °C and 5.5 GPa for 15 min (c) and (d) present high magnification images of dense and porous matrix in T800, respectively.



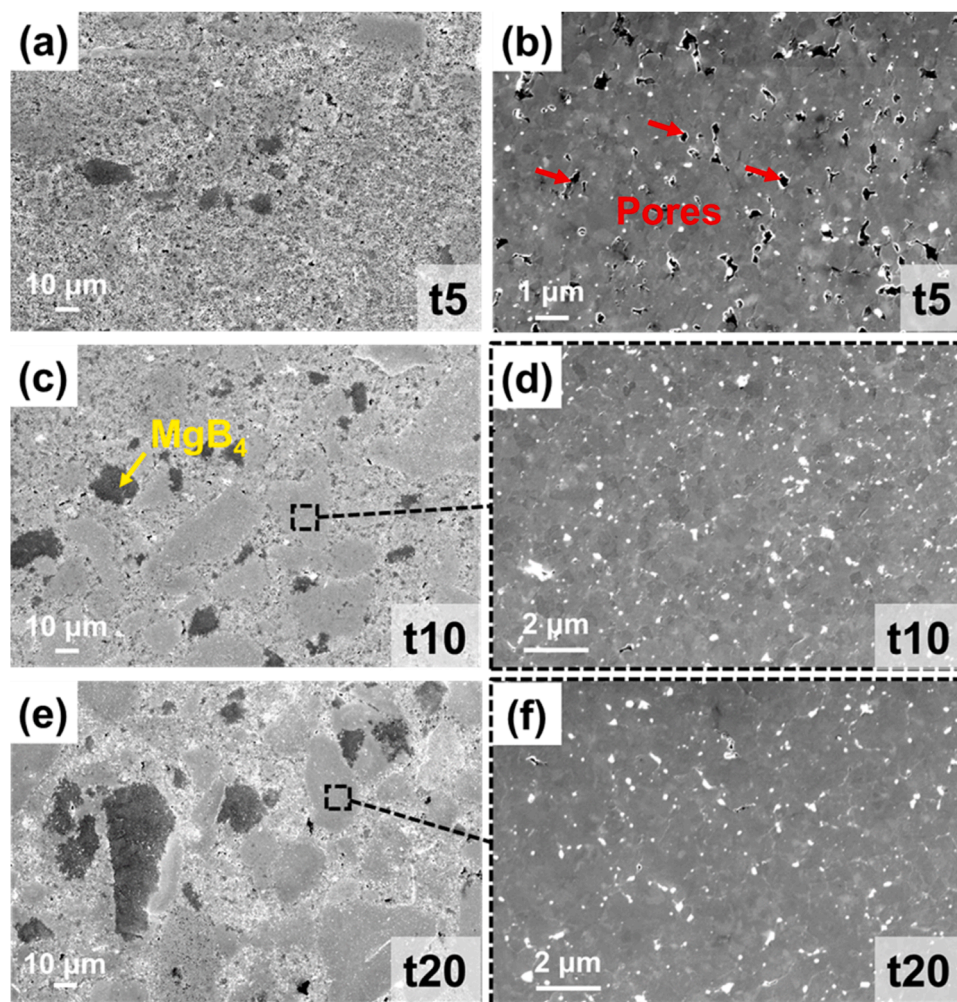


**Fig. 4.** SEM images of (a) t5, (b) t10 and (c) t20 prepared under 5.5 GPa and at 800 °C. (d-f) are corresponding micrographs in dense MgB<sub>2</sub> regions at high magnification.

### 3.3. Analysis of grain size and defects

Electron backscatter diffraction (EBSD) results (Fig. 6) show that there is no apparent texture in any of these bulk samples because the ultra-high pressure is applied by a cubic press rather than a uniaxial press. The grain sizes are smaller in T700, indicating limited grain growth at such a low temperature. The black regions represent unsolved pixels from pores. With increasing temperature, the decreasing areal fraction of black pixels shows the elimination of this porosity (Fig. 6b-d). However, inhomogeneous areas with different grain sizes are presented in Fig. 6e, labelled as A and B, where fine-grained matrix includes a higher amount of MgO impurities. The phase map obtained by TKD, as shown in Fig. 6f, demonstrates that the much smaller regions of unsolved pixels in Area B, that are beyond the resolution of traditional EBSD, come from the presence of nanograins of MgO and MgB<sub>4</sub>, or pores. A consistent picture of the microstructure emerges from imaging at the different length scales shown in Figs. 3 and 5, with dense aggregates of well-connected MgB<sub>2</sub> grains separated by regions containing a large number of small insulating phases. The average grain size distribution, as shown in Fig. 6g, displays, as expected, a steady increase with sintering temperature. The broader grain size distribution in both T900 and T1100 is a consequence of the mixture of small grains in the transition zones and larger grains in the well-connected regions.

It is well known that the grain size (density of grain boundaries) is critical to the performance of MgB<sub>2</sub> superconductors [36], but lattice defects such as dislocations can also introduce efficient flux pinning

centres [37]. The dislocation density was investigated by transmission electron microscopy (TEM), as shown in Fig. 7. Dense dislocation networks can easily be detected in both the Scanning TEM and High-resolution TEM images in T900, while the MgB<sub>2</sub> grains in T1100 are almost free of these defects. This observation is consistent with the XRD results in Table 2, demonstrating that micro-strain is almost fully released in the samples processed at higher temperatures.

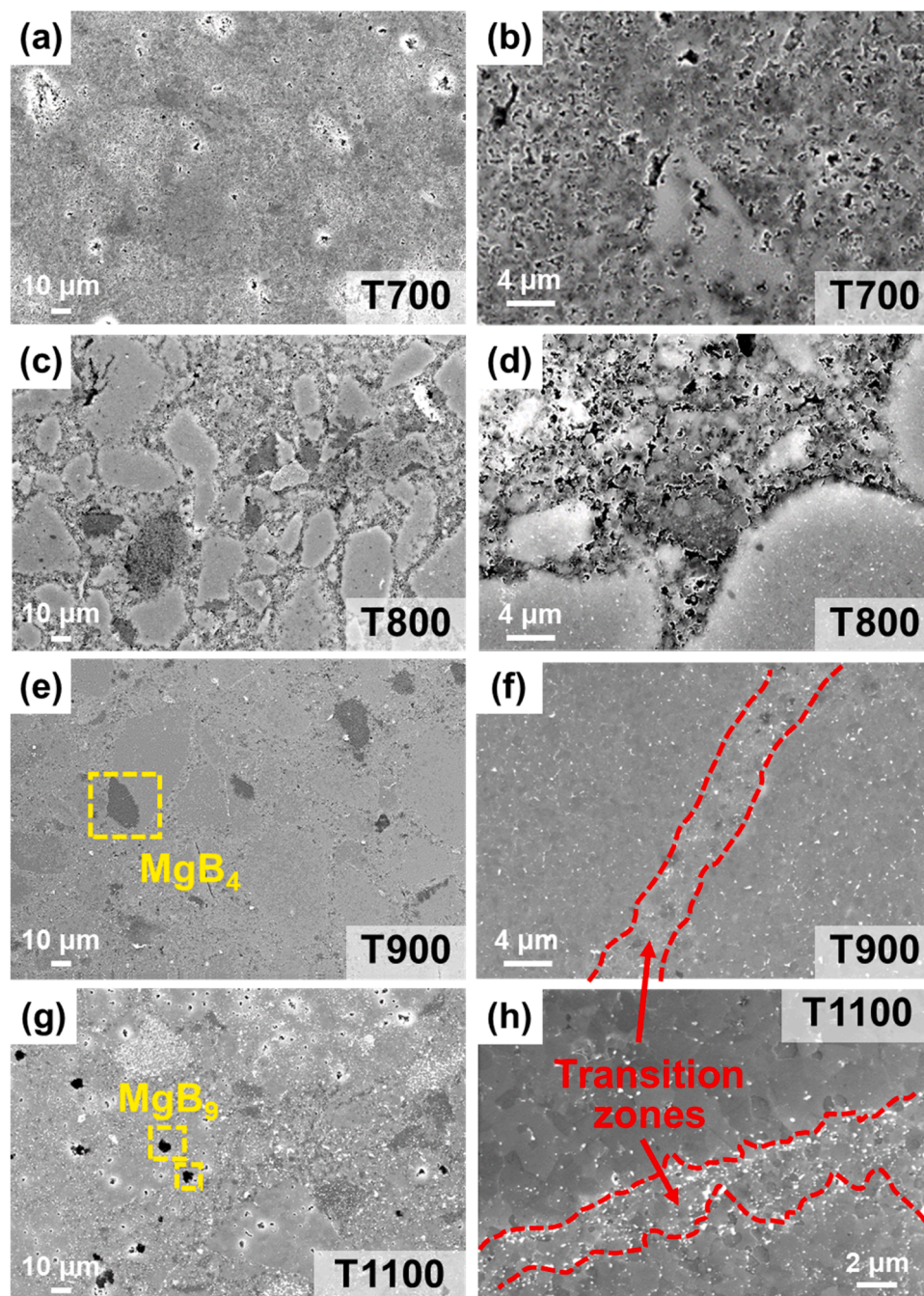
### 3.4. Superconducting properties

Fig. 8a shows the DC susceptibility of these MgB<sub>2</sub> bulk samples as a function of temperature. The onset  $T_c$  fluctuates in a narrow range between 38 K and 39 K, with the highest value being 38.7 K in T1100 compared with 38.2 K in T700.  $\Delta T$  becomes generally narrower with increasing processing temperature, with values around 2 K in T800 and over 15 K in T700. According to percolation theory, if the sample is homogeneous and free of microstructural defects like pores and impurities,  $\Delta T_a$  values due to anisotropy should change linearly with magnetic field as [13]:

$$\Delta T_a = \frac{\sqrt{(\gamma^2 - 1)p_c^2 + 1} - 1}{-\partial B_{c2}/\partial T} B$$

where  $\gamma$  represents the anisotropy. The percolation threshold  $p_c$  depends on the number of connections to neighboring grains [13], so samples with higher  $\gamma$  and  $p_c$  will have broader  $\Delta T$  values, and material





**Fig. 5.** Scanning electron microscopy (SEM) micrographs of samples processed at (a–b) 700 °C, (c–d) 800 °C, (e–f) 900 °C and (g–h) 1100 °C captured at 500× and 3000× magnifications, respectively.

inhomogeneities (lattice distortion, grain defects, or porosity) and thermal fluctuations can also lead to additional broadening [38]. The residual plastic deformation and porosity at low processing temperatures may be responsible for the two-step transition (grey arrows) in the susceptibility curve of T700. The loss of this feature in T800 indicates the lattice disorder is partially removed as the processing temperature increases to 800 °C.

$J_c$  values calculated by Bean's critical state model as a function of  $B_{app}$  obtained from magnetisation loops at 4.2 K and 20 K are shown in Fig. 8b and c. At both measurement temperatures, T900 performs best at both low and high magnetic fields. The  $J_c$  performance of T1100 in low field is comparable with that of T900, but  $J_c$  deteriorates much faster with increasing magnetic field. This deterioration is so severe in T1100 that the  $J_c(B_{app})$  curve of T800 crosses that of T1100 at around 4.5 T.

T700 has the lowest  $J_c$  values over the entire field range. For comparison, results from  $MgB_2$  samples processed under ultra-high pressures (>2 GPa) in other studies are included in Fig. 8d. Jin et al. pointed out that high pressure can prevent Mg evaporation at elevated temperatures and accelerates the reaction so the dwell time was reduced [26]. The study of Takano et al. has no corresponding microstructural characterization [27], but the shape of the  $J_c(B)$  curve of their ex-situ samples is similar to that of Jin et al. These samples have comparable low field  $J_c$  values to our T900 material, but decrease more rapidly as the field increases. Prikhna et al. have prepared both in-situ and ex-situ  $MgB_2$  samples with a wide range of  $J_c$  behaviours. The low-field  $J_c$  values in their in-situ samples can reach the very high value of  $2 \times 10^{10}$  A/m<sup>2</sup> at 0 T, which we assume indicates that the excellent inter-grain connectivity widely discussed for in-situ processed material is further improved



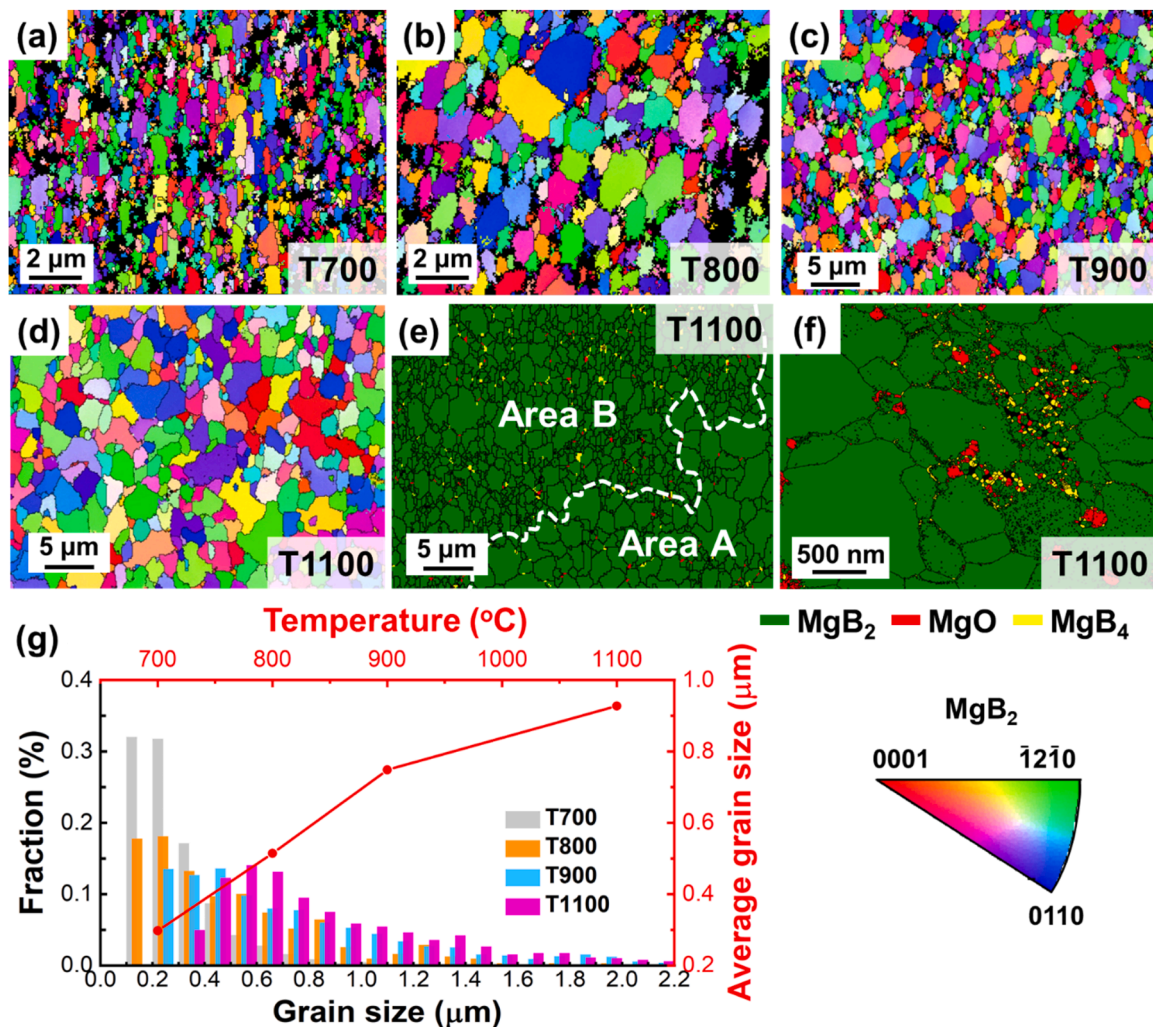


**Fig. 6.** EBSD IPF maps from samples produced at (a) 700 °C, (b) 800 °C, (c) 900 °C and (d) 1100 °C. The black grain boundaries represent misorientations larger than 15°. (e) and (f) are phase maps of T1100 taken by traditional EBSD and by TKD, respectively. (g) shows the average size distribution of MgB<sub>2</sub> grains in these samples.

by the high density achieved by high pressure synthesis. In contrast, most of their ex-situ samples without any flux pinning additions perform poorly over both low and high field ranges [29], apart from one ex-situ sample prepared at 1050 °C under 2 GPa that is reported in [39] to have an extremely high value of  $7 \times 10^9$  A/m<sup>2</sup> at 0 T and excellent high field performance as well. The authors attribute these surprisingly good properties to grain boundary pinning, but without direct evidence for the exceptionally fine grain size (<100 nm) that would be required to explain these remarkable results. The same authors performed systematic microstructural characterization on other samples, and concluded that nanostructural inhomogeneities such as Mg-B-O impurities and MgB<sub>x</sub> ( $x > 4$ ) inclusions served as effective pinning centres in in-situ samples, but these are not obviously present in the outstanding ex-situ sample [28]. They suggest that MgB<sub>12</sub> particles may be particularly effective flux pinning sites in samples [29,40], but high resolution analysis of the kind reported in Fig. 6f indicates that in our materials this phase is not present as a fine distribution of small particles necessary to have a strong influence on the high field properties.

Here we discuss how the microstructures presented above may control the magnetisation performance of our samples. Fig. 9 illustrates schematically how different sample microstructures can influence the length scale of circulating currents induced in magnetisation measurements, and hence the resultant magnetic moment measured. Firstly, processing at 900 °C results in almost complete densification, enabling

the superconducting current to circulate throughout the whole sample (Fig. 5f). The much better performance of T1100 compared with T800 in the low-field range is a result of its higher density. Secondly, the transition regions consisting of fine MgB<sub>2</sub> grains and MgO impurities, and shown in Fig. 5f and h, are important because they connect dense MgB<sub>2</sub> regions, thus controlling the macroscopic current flowing through the sample. As the processing temperature is increased, MgB<sub>2</sub> decomposition to produce insulating phases becomes more of a problem. The formation of MgB<sub>4</sub> grains (orange grains in Fig. 9) surrounding well-connected regions in T1100 severely inhibits macroscopic current flow. Once the bulk sample contains too many poorly connected layers (transition regions), the anisotropy of MgB<sub>2</sub> becomes an important factor [13]. Since the upper critical field of MgB<sub>2</sub> is much lower parallel to the c-axis than perpendicular, the current-carrying capacity of individual superconducting grains varies with the angle between the c axis and the direction of B<sub>app</sub>. Unfavourably aligned grains will lose their superconductivity in low magnetic fields, so the supercurrent has to divert around them. If the remaining MgB<sub>2</sub> grains in the passages are “switched-off” (black grains), currents will only circulate within the dense regions, contributing much less to the total ΔM, according to Bean’s critical state model, and thus leading to the much faster decrease in J<sub>c</sub> values in T1100 than in T900.

The intrinsic properties of MgB<sub>2</sub> are improved by the reduction of the grain size and the introduction of lattice defects, for instance by plastic



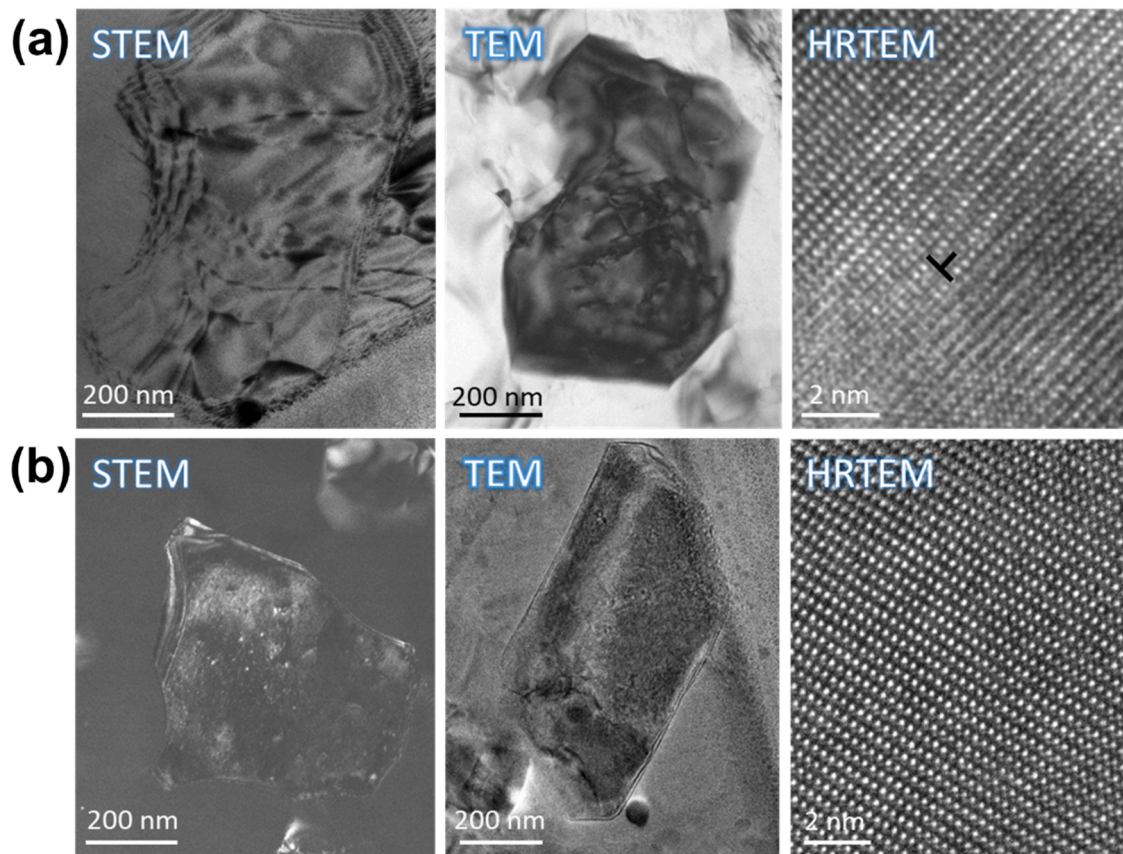


Fig. 7. Typical Scanning TEM, TEM and HRTEM images of  $\text{MgB}_2$  grains in (a) T900 and (b) T1100 samples.

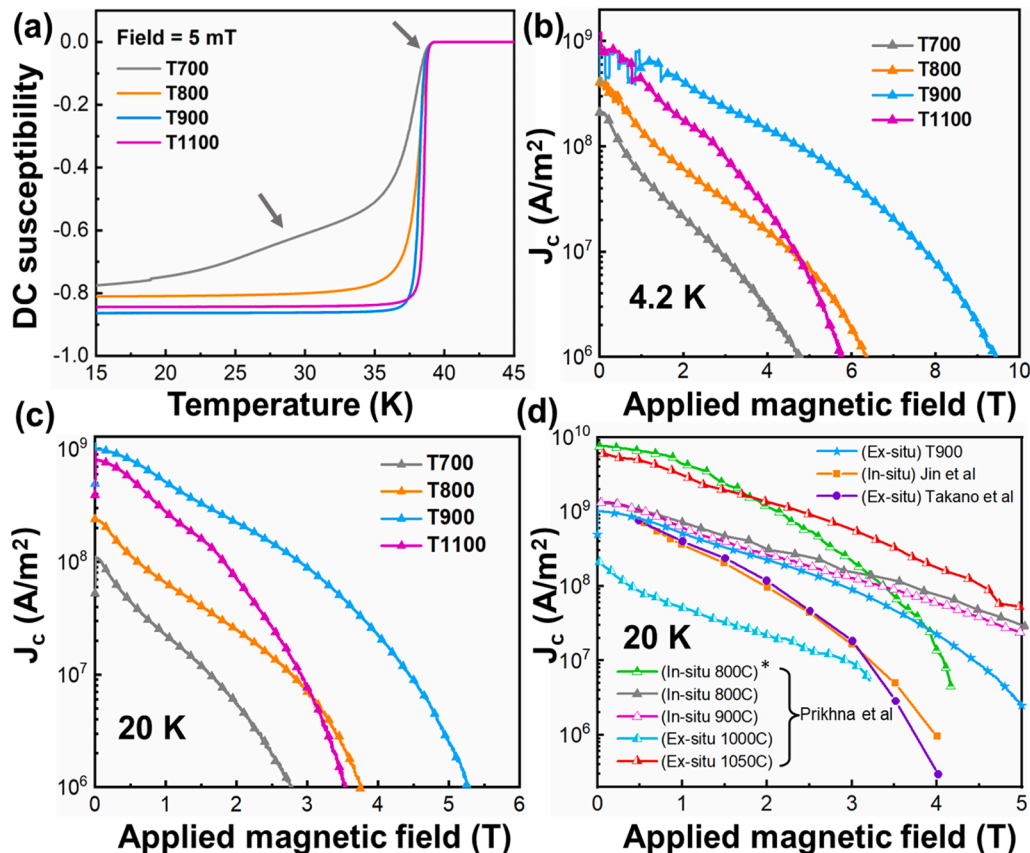
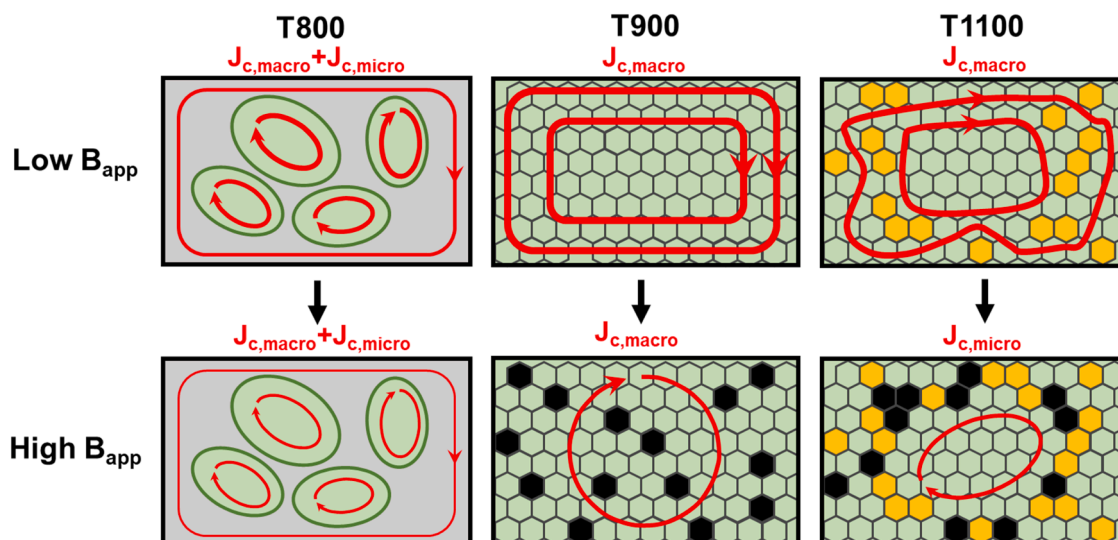


Fig. 8. (a) DC susceptibility curves of bulk samples in the temperature series measured under 5 mT. (b) and (c) present  $J(B_{\text{app}})$  curves of T700, T800, T900 and T1100 at 4.2 K and 20 K. (d) The performance of T900 is compared to other undoped  $\text{MgB}_2$  samples in the literature synthesised at high pressures: in-situ  $\text{MgB}_2$  samples prepared at 900 °C under 3 GPa for 10 min (Jin et al. [26]), ex-situ  $\text{MgB}_2$  samples prepared at 1000 °C under 3.5 GPa for 2 h (Takano et al. [27]), in-situ  $\text{MgB}_2$  samples prepared at 800 °C and 900 °C under 2 GPa for 1 h (Prikhna et al. [29]), and ex-situ  $\text{MgB}_2$  samples prepared at 1000 °C and 1050 °C under 2 GPa for 1 h (Prikhna et al. [28,39,40]) are included. The star is used to distinguish in-situ samples prepared from different boron starting powder.



**Fig. 9.** Schematics of circulating currents in three different microstructures representing the T800, T900 and T1100 samples in low and high magnetic fields. Green regions represent dense, well-connected  $\text{MgB}_2$  regions and grey regions are porous. Black grains represent  $\text{MgB}_2$  grains oriented such that they can be “switched-off” by the applied magnetic field, and orange represents  $\text{MgB}_4$  grains.

deformation. Since processing at 900 °C does not fully anneal out defects like dislocations that are able to act as pinning centres nor leads to rapid grain growth (Fig. 7a), the T900 sample has the best high-field superconducting performance. However, the higher temperature processing of T1100 leads to the annealing out of lattice defects and encourages significant grain growth, so it is understandable that the pinning strength is substantially reduced, leading to poorer performance. The worst  $J_c$  behaviour of T700 is attributed to both high porosity and poor grain connectivity, which means that there are no large supercurrent loops [17].

#### 4. Conclusions

High-density nanostructured  $\text{MgB}_2$  samples have been fabricated by ultra-high pressure-assisted sintering. The effect of temperature has been systematically examined, and the following conclusions can be drawn:

- For processing nanostructured, dense  $\text{MgB}_2$  bulk samples, ultra-high pressure is beneficial for shortening the sintering time to 15 min (compared to several hours in methods such as the powder-in-closed-tube method [41]). Complete densification can be achieved at a relatively low processing temperature of 900 °C.
- Ultra-high pressure can inhibit the decomposition of  $\text{MgB}_2$  compared with the field-assisted sintering technology (Table 2), and also introduces lattice defects such as dislocations. However, the number of impurity phases still increases with higher processing temperatures due to more severe  $\text{MgB}_2$  decomposition. The  $\text{MgB}_2$  grains grow rapidly and lattice defects are fully annealed out when the processing temperature is over 1100 °C.
- $T_c$  and  $\Delta T$  values are both degraded at the lower processing temperatures because of the lattice distortion from plastic deformation (dislocations). The sample density also influences the low-field performance, so T1100 has comparable  $J_c$  performance with T900 at low fields.
- Smaller grain sizes and the presence of grain defects can increase the pinning density, which influences the high-field performance in samples processed at low temperatures. However,  $\text{MgB}_4$  grains are formed at higher temperatures, and affect the interconnection between dense  $\text{MgB}_2$  regions which influences the availability of the paths for macroscopic currents in high magnetic fields. As a

consequence, both T800 and T900 outperform T1100 in high magnetic fields, and an intermediate temperature gives the best combination of properties at both high and low fields.

- In our samples, the best superconducting properties are achieved using a processing temperature of 900 °C. The  $J_c$  value in 5 T is the highest of those reported for ex-situ samples prepared by ultra-high pressure-assisted sintering (except for one sample in [40]), and is superior to most in-situ samples prepared by other methods as well. Therefore, we propose that an effective set of conditions to prepare high performance  $\text{MgB}_2$  bulks from pre-reacted powder are 5 GPa for the applied pressure, 900 °C for the processing temperature and 15 min for the processing time.

#### Declaration of Competing Interest

The authors declare that they have no known competing financial interests or personal relationships that could have appeared to influence the work reported in this paper.

#### Acknowledgements

The authors gratefully acknowledge the UK Engineering and Physical Science Research Council for the financial support (EP/P026427) and Element Six Company for sample preparation. David Cockayne Centre for Electron is acknowledged for providing characterisation facilities.

#### Appendix A. Supporting information

Supplementary data associated with this article can be found in the online version at [doi:10.1016/j.jeurceramsoc.2022.09.008](https://doi.org/10.1016/j.jeurceramsoc.2022.09.008).

#### References

- J.H. Durrell, M.D. Ainslie, D. Zhou, P. Vanderbemden, T. Bradshaw, S. Speller, M. Filipenko, D.A. Cardwell, Bulk superconductors: a roadmap to applications, *Supercond. Sci. Technol.* 31 (10) (2018), <https://doi.org/10.1088/1361-6668/aad7ce>.
- J. Nagamatsu, N. Nakagawa, T. Muranaka, Y. Zenitani, J. Akimitsu, Superconductivity at 39 K in magnesium diboride, *Nature* 410 (2001) 63, <https://doi.org/10.1038/35065039>.
- J.H. Durrell, M.D. Ainslie, D. Zhou, P. Vanderbemden, T. Bradshaw, S. Speller, M. Filipenko, D.A. Cardwell, Bulk superconductors: a roadmap to applications, *Supercond. Sci. Technol.* 31 (10) (2018), 103501, <https://doi.org/10.1088/1361-6668/aad7ce>.

- [4] P. Mikheenko, E. Martínez, A. Bevan, J.S. Abell, J.L. MacManus-Driscoll, Grain boundaries and pinning in bulk  $\text{MgB}_2$ , *Supercond. Sci. Technol.* 20 (9) (2007) S264–S270, <https://doi.org/10.1088/0953-2048/20/9/s22>.
- [5] D.C. Larbalestier, L.D. Cooley, M.O. Rikel, A.A. Polyanski, J. Jiang, S. Patnaik, X. Y. Cai, D.M. Feldmann, A. Gurevich, A.A. Squitieri, M.T. Naus, C.B. Eom, E. Hellstrom, R.J. Cava, K.A. Regan, N. Rogado, M.A. Hayward, T. He, J.S. Slusky, P. Khalifah, K. Inumaru, M. Haas, Strongly linked current flow in polycrystalline forms of the superconductor  $\text{MgB}_2$ , *Nature* 410 (6825) (2001) 186–189, <https://doi.org/10.1038/35065559>.
- [6] J. Zou, M.D. Ainslie, H. Fujishiro, A.G. Bhagurkar, T. Naito, N. Hari Babu, J. F. Fagnard, P. Vanderbemden, A. Yamamoto, Numerical modelling and comparison of  $\text{MgB}_2$  bulks fabricated by HIP and infiltration growth, *Supercond. Sci. Technol.* 28 (7) (2015), <https://doi.org/10.1088/0953-2048/28/7/075009>.
- [7] A. Gümbel, J. Eckert, G. Fuchs, K. Nenkov, K.H. Müller, L. Schultz, Improved superconducting properties in nanocrystalline bulk  $\text{MgB}_2$ , *Appl. Phys. Lett.* 80 (15) (2002) 2725–2727, <https://doi.org/10.1063/1.1469654>.
- [8] G. Fuchs, W. Häbeler, K. Nenkov, J. Scheiter, O. Perner, A. Handstein, T. Kanai, L. Schultz, B. Holzapfel, High trapped fields in bulk  $\text{MgB}_2$  prepared by hot-pressing of ball-milled precursor powder, *Supercond. Sci. Technol.* 26 (12) (2013), 122002, <https://doi.org/10.1088/0953-2048/26/12/122002>.
- [9] S. Sugino, A. Yamamoto, J.-i Shimoyama, K. Kishio, Enhanced trapped field in  $\text{MgB}_2$  bulk magnets by tuning grain boundary pinning through milling, *Supercond. Sci. Technol.* 28 (5) (2015), 055016, <https://doi.org/10.1088/0953-2048/28/5/055016>.
- [10] S. Mizutani, A. Yamamoto, J.I. Shimoyama, H. Ogino, K. Kishio, Self-sintering-assisted high intergranular connectivity in ball-milled ex situ  $\text{MgB}_2$  bulks, *Supercond. Sci. Technol.* 27 (11) (2014), <https://doi.org/10.1088/0953-2048/27/11/114001>.
- [11] Y. Zhao, D.X. Huang, Y. Feng, C.H. Cheng, T. Machi, N. Koshizuka, M. Murakami, Nanoparticle structure of  $\text{MgB}_2$  with ultrathin  $\text{TiB}_2$  grain boundaries, *Appl. Phys. Lett.* 80 (9) (2002) 1640–1642, <https://doi.org/10.1063/1.1456969>.
- [12] W. Pachla, P. Kov, C. R. Didusko, A. Mazur, I. Hušek, A. Morawski, A. Presz, Effects of the high-pressure treatment of ex situ  $\text{MgB}_2$  superconductors, *Supercond. Sci. Technol.* 16 (1) (2002) 7–13, <https://doi.org/10.1088/0953-2048/16/1/302>.
- [13] M. Eisterer, M. Zehetmayer, H.W. Weber, Current percolation and anisotropy in polycrystalline  $\text{MgB}_2$ , *Phys. Rev. Lett.* 90 (24) (2003), 247002, <https://doi.org/10.1103/PhysRevLett.90.247002>.
- [14] A. Yamamoto, H. Tanaka, J.-i Shimoyama, H. Ogino, K. Kishio, T. Matsushita, Towards the realization of higher connectivity in  $\text{MgB}_2$  conductors: In-situ or sintered ex-situ? *Jpn. J. Appl. Phys.* 51 (1) (2012) <https://doi.org/10.1143/jjap.51.010105>.
- [15] C.E.J. Dancer, D. Prabhakaran, M. Başoğlu, E. Yanmaz, H. Yan, M. Reece, R. I. Todd, C.R.M. Grovenor, Fabrication and properties of dense ex situ magnesium diboride bulk material synthesized using spark plasma sintering, *Supercond. Sci. Technol.* 22 (9) (2009), 095003, <https://doi.org/10.1088/0953-2048/22/9/095003>.
- [16] G. Aldica, D. Batalu, S. Popa, I. Ivan, P. Nita, Y. Sakka, O. Vasyukiv, L. Miu, I. Pasuk, P. Badica, Spark plasma sintering of  $\text{MgB}_2$  in the two-temperature route, *Phys. C: Supercond.* 477 (2012) 43–50, <https://doi.org/10.1016/j.physc.2012.01.023>.
- [17] G.A.B. Matthews, S. Santra, R. Ma, C.R.M. Grovenor, P.S. Grant, S.C. Speller, Effect of the sintering temperature on the microstructure and superconducting properties of  $\text{MgB}_2$  bulks manufactured by the field assisted sintering technique, *Supercond. Sci. Technol.* 33 (5) (2020), <https://doi.org/10.1088/1361-6668/ab7c53>.
- [18] J.Y. Zhang, Y.F. Zhang, Z.W. Lou, P.H. Zhang, C.Y. Li, J.W. Yuan, L. Peng, Y.X. Ma, J.G. Noudem, M. Izumi, The discrepancies in different facets of  $\text{MgB}_2$  bulk superconductors prepared under various sintering durations by spark plasma sintering, *Supercond. Sci. Technol.* 34 (4) (2021), 045011, <https://doi.org/10.1088/1361-6668/abe3f2>.
- [19] T. Naito, Y. Endo, H. Fujishiro, Optimization of vortex pinning at grain boundaries on ex-situ  $\text{MgB}_2$  bulks synthesized by spark plasma sintering, *Supercond. Sci. Technol.* 30 (9) (2017), <https://doi.org/10.1088/1361-6668/aa6d14>.
- [20] A. Mesquita, M.I.B. Bernardi, V.R. Mastelaro, M.H. Lente, J.A. Eiras, M.R. Gallas, T. M.H. Costa, Nanograined ferroelectric ceramics prepared by high-pressure densification technique, *J. Am. Ceram. Soc.* 92 (8) (2009) 1679–1683, <https://doi.org/10.1111/j.1551-2916.2009.03083.x>.
- [21] D. Lahiri, V. Singh, G.R. Rodrigues, T.M.H. Costa, M.R. Gallas, S.R. Bakshi, S. Seal, A. Agarwal, Ultra high-pressure consolidation and deformation of tantalum carbide at ambient and high temperatures, *Acta Mater.* 61 (11) (2013) 4001–4009, <https://doi.org/10.1016/j.actamat.2013.03.014>.
- [22] J. Gu, J. Zou, J. Liu, H. Wang, J. Zhang, W. Wang, Z. Fu, Sintering highly dense ultra-high temperature ceramics with suppressed grain growth, *J. Eur. Ceram. Soc.* 40 (4) (2020) 1086–1092, <https://doi.org/10.1016/j.jeurceramsoc.2019.11.056>.
- [23] B. Matovic, F. Zivic, S. Mitrovic, D. Prsic, V. Maksimovic, T. Volkov-Husovic, R. Kumar, N. Daneu, Ultra-high pressure densification and properties of nanostructured  $\text{SiC}$ , *Mater. Lett.* 164 (2016) 68–71, <https://doi.org/10.1016/j.matlet.2015.09.043>.
- [24] L. Liu, X. Li, Q. He, L. Xu, X. Cao, X. Peng, C. Meng, W. Wang, W. Zhu, Y. Wang, Sintering dense boron carbide without grain growth under high pressure, *J. Am. Ceram. Soc.* 101 (3) (2018) 1289–1297, <https://doi.org/10.1111/jace.15282>.
- [25] F. Liu, D. He, P. Liu, H. Wang, C. Xu, S. Yin, W. Yin, Y. Li, Plastic deformation and sintering of alumina under high pressure, *J. Appl. Phys.* 114 (23) (2013), 233504, <https://doi.org/10.1063/1.4844495>.
- [26] C.Q. Jin, S.C. Li, J.L. Zhu, F.Y. Li, Z.X. Liu, R.C. Yu, High critical current density of a  $\text{MgB}_2$  bulk superconductor high-pressure synthesized directly from the elements, *J. Mater. Res.* 17 (3) (2002) 525–527, <https://doi.org/10.1557/JMR.2002.0073>.
- [27] Y. Takano, H. Takeya, H. Fujii, H. Kumakura, T. Hatano, K. Togano, H. Kito, H. Ihara, Superconducting properties of  $\text{MgB}_2$  bulk materials prepared by high-pressure sintering, *Appl. Phys. Lett.* 78 (19) (2001) 2914–2916, <https://doi.org/10.1063/1.1371239>.
- [28] T. Prikhna, W. Gawalek, Y. Savchuk, V. Tkach, N. Danilenko, M. Wendt, J. Dellith, H. Weber, M. Eisterer, V. Moshchil, N. Sergienko, A. Kozyrev, P. Nagorny, A. Shapovalov, V. Melnikov, S. Dub, D. Litzkendorf, T. Habisreuther, C. Schmidt, A. Mamalis, V. Sokolovsky, V. Sverdun, F. Karau, A. Starostina, Higher borides and oxygen-enriched Mg–B–O inclusions as possible pinning centers in nanostructural magnesium diboride and the influence of additives on their formation, *Phys. C: Supercond.* 470 (19) (2010) 935–938, <https://doi.org/10.1016/j.physc.2010.02.064>.
- [29] T.A. Prikhna, W. Gawalek, Y.M. Savchuk, T. Habisreuther, M. Wendt, N. V. Sergienko, V.E. Moshchil, P. Nagorny, C. Schmidt, J. Dellith, U. Dittrich, D. Litzkendorf, V.S. Melnikov, V.B. Sverdun, The inclusions of Mg–B ( $\text{MgB}_{12}$ ?) as potential pinning centres in high-pressure-high-temperature-synthesized or sintered magnesium diboride, *Supercond. Sci. Technol.* 20 (9) (2007) S257–S263, <https://doi.org/10.1088/0953-2048/20/9/s21>.
- [30] Element Six (UK) Ltd. 2022; Available from: <https://www.e6.com/en>.
- [31] R. Prozorov, V.G. Kogan, Effective demagnetizing factors of diamagnetic samples of various shapes, *Phys. Rev. Appl.* 10 (1) (2018), <https://doi.org/10.1103/PhysRevApplied.10.014030>.
- [32] S. Brutti, A. Ciccio, G. Balducci, G. Gigli, P. Manfrinetti, A. Palenzona, Vaporization thermodynamics of  $\text{MgB}_2$  and  $\text{MgB}_4$ , *Appl. Phys. Lett.* 80 (16) (2002) 2892–2894, <https://doi.org/10.1063/1.1471382>.
- [33] J. Nagamatsu, N. Nakagawa, T. Muranaka, Y. Zenitani, J. Akimitsu, Superconductivity at 39 K in magnesium diboride, *Nature* 410 (6824) (2001) 63–64, <https://doi.org/10.1038/35065039>.
- [34] S.D. Bohnenstiehl, M.A. Susner, S.A. Dregia, M.D. Sumption, J. Donovan, E. W. Collings, Experimental determination of the peritectic transition temperature of  $\text{MgB}_2$  in the Mg–B phase diagram, *Thermochim. Acta* 576 (2014) 27–35, <https://doi.org/10.1016/j.tca.2013.11.027>.
- [35] S. Kim, D.S. Stone, J.-I. Cho, C.-Y. Jeong, C.-S. Kang, J.-C. Bae, Phase stability determination of the Mg–B binary system using the CALPHAD method and ab initio calculations, *J. Alloy. Compd.* 470 (1–2) (2009) 85–89, <https://doi.org/10.1016/j.jallcom.2008.02.099>.
- [36] E. Martínez, P. Mikheenko, M. Martínez-López, A. Millán, A. Bevan, J.S. Abell, Flux pinning force in bulk  $\text{MgB}_2$  with variable grain size, *Phys. Rev. B* 75 (13) (2007), 134515, <https://doi.org/10.1103/PhysRevB.75.134515>.
- [37] S. Li, T. White, K. Laursen, T.T. Tan, C.Q. Sun, Z.L. Dong, Y. Li, S.H. Zho, J. Horvat, S.X. Dou, Intense vortex pinning enhanced by semicrystalline defect traps in self-aligned nanostructured  $\text{MgB}_2$ , *Appl. Phys. Lett.* 83 (2) (2003) 314–316, <https://doi.org/10.1063/1.1591070>.
- [38] C.C. Wang, R. Zeng, X. Xu, S.X. Dou, Superconducting transition width under magnetic field in  $\text{MgB}_2$  polycrystalline samples, *J. Appl. Phys.* 108 (9) (2010), <https://doi.org/10.1063/1.3488631>.
- [39] T. Prikhna, W. Gawalek, Y. Savchuk, A. Soldatov, V. Sokolovsky, M. Eisterer, H. W. Weber, J. Noudem, M. Serga, V. Turkevich, M. Tompsic, V. Tkach, N. Danilenko, W. Goldacker, F. Karau, I. Fesenko, M. Rindfleisch, J. Dellith, M. Wendt, S. You, V. Meerovich, S. Dub, V. Moshchil, N. Sergienko, A. Kozyrev, T. Habisreuther, C. Schmidt, D. Litzkendorf, P. Nagorny, V. Sverdun, Effects of high pressure on the physical properties of  $\text{MgB}_2$ , *J. Supercond. Nov. Magn.* 24 (1–2) (2010) 137–150, <https://doi.org/10.1007/s10948-010-0909-3>.
- [40] T. Prikhna, W. Gawalek, M. Eisterer, H.W. Weber, M. Monastyrkov, V. Sokolovsky, J. Noudem, V. Moshchil, M. Karpets, V. Kovylae, A. Borimskiy, V. Tkach, A. Kozyrev, R. Kuznetsov, J. Dellith, C. Schmidt, D. Litzkendorf, F. Karau, U. Dittrich, M. Tomsic, The effect of high-pressure synthesis on flux pinning in  $\text{MgB}_2$ -based superconductors, *Phys. C: Supercond.* 479 (2012) 111–114, <https://doi.org/10.1016/j.physc.2012.01.004>.
- [41] Y. Shimada, S. Hata, K.-i Ikeda, H. Nakashima, S. Matsumura, H. Tanaka, A. Yamamoto, J.-i Shimoyama, K. Kishio, Microstructural connectivity in sintered ex-situ  $\text{MgB}_2$  bulk superconductors, *J. Alloy. Compd.* 656 (2016) 172–180, <https://doi.org/10.1016/j.jallcom.2015.09.253>.